ARTICLES
PUBLISHED ONLINE: 21 MARCH 2016 | DOI: 10.1038/NCHEM.2472

nature chemistry

Self-assembly of size-controlled liposomes on DNA nanotemplates

Yang Yang[1,2†], Jing Wang[1,2†], Hideki Shigematsu[3‡], Weiming Xu[1,2], William M. Shih[4,5,6*], James E. Rothman[1,2*] and Chenxiang Lin[1,2*]

Artificial lipid-bilayer membranes are valuable tools for the study of membrane structure and dynamics. For applications such as the study of vesicular transport and drug delivery, there is a pressing need for artificial vesicles with controlled size. However, controlling vesicle size and shape with nanometre precision is challenging, and approaches to achieve this can be heavily affected by lipid composition. Here, we present a bio-inspired templating method to generate highly monodispersed sub-100-nm unilamellar vesicles, where liposome self-assembly was nucleated and confined inside rigid DNA nanotemplates. Using this method, we produce homogeneous liposomes with four distinct predefined sizes. We also show that the method can be used with a variety of lipid compositions and probe the mechanism of templated liposome formation by capturing key intermediates during membrane self-assembly. The DNA nanotemplating strategy represents a conceptually novel way to guide lipid bilayer formation and could be generalized to engineer complex membrane/protein structures with nanoscale precision.

Cell membranes are tremendously complex in structure and function. They define cellular compartments and mediate biomolecule transport. A central task of cell biology is to elucidate the interplay between lipid bilayers and other molecules (for example, protein) that drive membrane dynamics and govern cell behaviour[1]. The use of an artificial membrane with well-defined properties is a powerful approach to analysing sophisticated cellular machinery in a controlled system with reduced complexity[2]. Engineering a customized lipid bilayer membrane is also an intriguing goal in biotechnology, and can open up opportunities such as drug delivery and biosensing[3–5].

An abundance of methods have been developed to create artificial membranes, especially in the form of unilamellar vesicles[6,7]. The manufacture of lipid vesicles generally includes the following three steps. First, lipids are dissolved in a good solvent (for example, oil, chloroform, aqueous solution with detergent), in which they are dispersed as single molecules or small aggregates (for example, micelles). Second, the lipids are transferred into a detergent-free aqueous solution to allow the self-assembly of bilayer membranes, which eventually form vesicles. This can be achieved in a number of ways, including steps of drying/rehydration, dialysis and reverse-phase evaporation[8–11]. Tuning the experimental conditions at this stage can often be effective for the generation of vesicles with desired properties[12–16]. Third, an external force (for example, sonication or extrusion) can be applied to the vesicles to control their size and improve the monodispersity[17–20]. However, despite the breakthroughs in producing vesicles with controlled geometry and surface chemistry, existing techniques suffer from one or more of the following limitations: (1) it remains a challenge to control the vesicle size (let alone the shape) with nanometre precision; (2) the experimental conditions required for a specific vesicle type are often empirically determined and may suffer from batch-to-batch differences; (3) some size-control methods depend heavily on lipid composition, which limits their adaptability[12]; (4) certain techniques entail the use of specialized types of experimental apparatus that are not readily available to a normal biochemistry laboratory[21–23].

Inspired by the protein machineries that sculpt and scaffold membrane structures in cells[24], a reasonable hypothesis is that high-precision membrane engineering can be achieved *in vitro* by applying a similar templating approach[25]. DNA has already been demonstrated to be a nanoscale material capable of gluing and fusing pre-assembled liposomes[26–28]. To generate programmable nanotemplates for vesicles, we therefore took advantage of an emerging technique termed 'structural DNA nanotechnology'[29,30]. Through the rational design of DNA-strand hybridization, this technique generates self-assembled nanostructures with programmable geometry, addressable surface and outstanding structural stability. More specifically, we used the 'DNA-origami'[31,32] technique to fold a single-stranded DNA (scaffold strand) into a customized shape with the help of many DNA oligonucleotides (staple strands). We then decorated the interior surface of the DNA-origami nanostructures with lipid molecules and used them to guide the formation of liposomes. In this way, we were able to obtain a series of highly monodispersed liposomes with sizes designed to be 29, 46, 60 and 94 nm. The methods also worked nicely for a variety of lipid compositions. Although others have successfully produced vesicles with artificial templates surrounded by membranes (that is, an endoskeleton)[33–35], our method differs in that the DNA nanostructure works as the 'exoskeleton' and generates vesicles with controlled size over a wider range and potentially with more versatile functions. Furthermore, this system provides a

[1]Department of Cell Biology, Yale University School of Medicine, New Haven, Connecticut 06520, USA. [2]Nanobiology Institute, Yale University, West Haven, Connecticut 06516, USA. [3]Department of Cellular and Molecular Physiology, Yale University School of Medicine, New Haven, Connecticut 06250, USA. [4]Wyss Institute for Biologically Inspired Engineering, Harvard University, Cambridge, Massachusetts 02138, USA. [5]Department of Biological Chemistry and Molecular Pharmacology, Harvard Medical School, Boston, Massachusetts 02115, USA. [6]Department of Cancer Biology, Dana-Farber Cancer Institute, Boston, Massachusetts 02215, USA. ‡Present address: Division of Structural and Synthetic Biology, RIKEN Center for Life Science Technologies, Yokohama, Kangawa 230-0045, Japan. †These authors contributed equally to this work. *e-mail: chenxiang.lin@yale.edu; james.rothman@yale.edu; william_shih@dfci.harvard.edu

© 2016 Macmillan Publishers Limited. All rights reserved

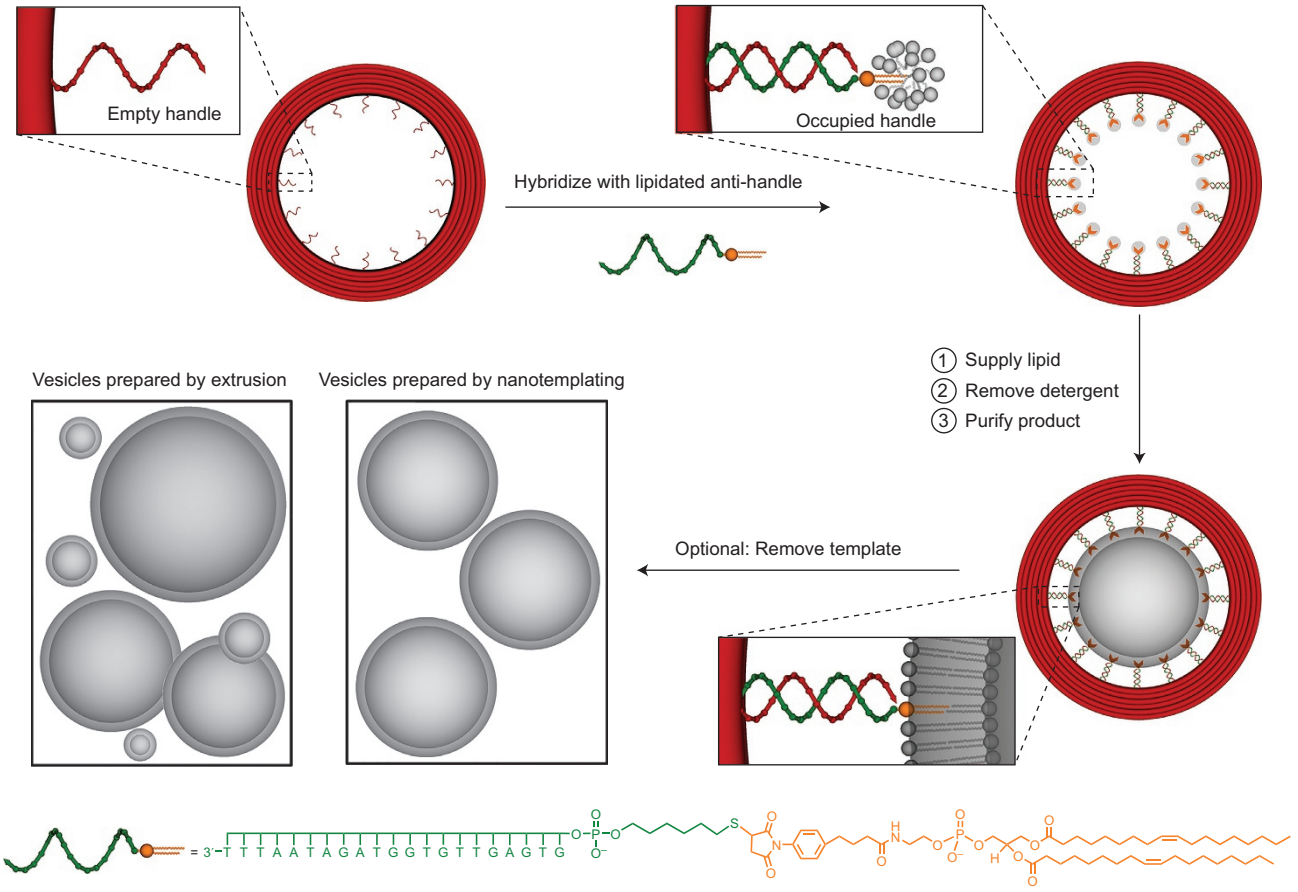


Figure 1 | Scheme for generating size-controlled vesicles by nanotemplating. A DNA-origami ring (red) carrying multiple single-stranded extensions (empty handles) is first constructed. DNA anti-handles (oligonucleotides with complementary sequence to handles) are chemically conjugated to DOPE and incubated with the DNA ring to allow hybridization. The chemical structure of the lipidated anti-handle (green curl with orange head) is shown at the bottom. Third, the ring with occupied handles is mixed with extra lipid and detergent, and dialysed to allow vesicle formation. The desired product (liposomes, with their size determined by the DNA template) is purified via isopycnic centrifugation. Finally, the vesicles (grey bubbles) can be released from the DNA ring, giving rise to a pool of liposomes with better homogeneity than those prepared by traditional methods such as extrusion.

unique tool for studying nucleated lipid assembly into a liposome within a rigid template. We studied the mechanism of this templated vesicle formation by capturing critical intermediates during the bilayer self-assembly.

Results

We designed four different DNA-origami rings (Supplementary Fig. 1) and used them as templates to define the liposome size. The scheme for this DNA-ring templated liposome production is presented in Fig. 1. Taking a 12-helix-bundle ring with 60 nm inner diameter, for example, a DNA ring was assembled by mixing an 8,064-nucleotide (nt) scaffold strand and 225 staple strands in a molar ratio of 1:6 followed by 36 h of thermal annealing and purification by rate-zonal centrifugation[36] (Supplementary Fig. 2). A well-folded ring carried sixteen 21-nt single-stranded DNA handles spaced evenly along an inner DNA helix and pointing towards the centre of the ring. It also carried eight evenly spaced outer handles (not shown in Fig. 1 for clarity; for more details see Supplementary Fig. 3). The inner and outer handles were designed to have orthogonal sequences. A thiol-modified DNA strand complementary to the inner handle (anti-inner handle) was chemically conjugated with 1,2-dioleoyl-*sn*-glycero-3-phosphoethanolamine-*N*-[4-(*p*-maleimidophenyl)butyramide] (18:1 MPB PE) via a thiol-maleimide crosslinking reaction. To label the DNA rings with fluorescently modified anti-outer handles and lipidated anti-inner handles, rings were mixed with an excessive amount of anti-handles in a solution containing 1% *n*-octyl-β-D-glucopyranoside (OG) to allow for hybridization. The fluorescently labelled DNA ring–lipid complex was subsequently mixed with extruded liposomes (~1:188,000 ring-to-lipid molar ratio) in a solution containing OG at its critical micelle formation concentration (CMC) of 0.67% (wt/vol). The solution was then dialysed for 16 h to allow for detergent removal and liposome formation. Finally, the detergent-free solution was loaded onto an iodixanol gradient and spun in an ultracentrifuge to separate the crude products based on their buoyant density.

The first method we used to characterize our product was gel electrophoresis. As shown in Fig. 2a, fractions collected after isopycnic centrifugation were resolved on an agarose gel with 0.05% SDS, which served to disrupt membranes into lipid–detergent micelles. Because the DNA rings and membranes were labelled with cyanine-5 (Cy5)-modified anti-outer handle and rhodamine(B)-PE (Rhod-PE), respectively, they fluoresced in two separate channels (pseudo-coloured green and red). The first fraction (least dense, F1) contained only free lipid aggregates, without any DNA rings. In the second to seventh fractions (F2–F7), DNA rings coexisted with lipids, suggesting the formation of DNA–ring associated vesicles. The denser fractions (F8–F12) contained neither DNA nor lipid. In contrast, in the absence of inner handle and/or lipid-modified anti-inner handle (Supplementary Fig. 4), F8–F12 contained only DNA rings and F1–F7 contained only lipids. Therefore, the association between DNA ring and lipid in the final product depends

© 2016 Macmillan Publishers Limited. All rights reserved

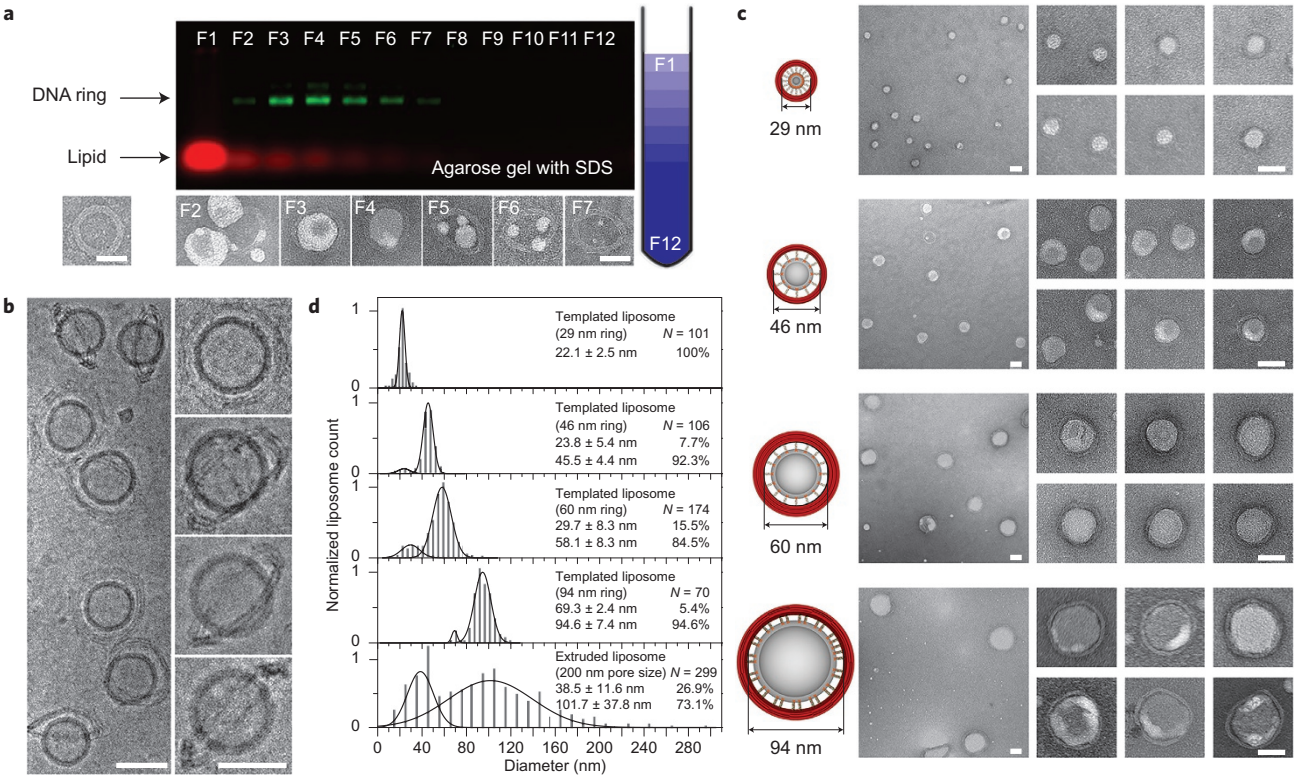


Figure 2 | Characterization of DNA-templated liposomes. a, General workflow: resolving the density gradient fractions by agarose gel electrophoresis and imaging the fractions with TEM. Fractions are numbered sequentially from F1 to F12 from the top to the bottom of the gradient. A typical gel image is shown, together with representative TEM images of F2–F7. A lipid-free 60 nm DNA ring is also shown for comparison. Note that the Cy5-labelled DNA ring and rhodamine(B)-labelled lipid ran as two separate bands due to the presence of SDS during electrophoresis. **b**, Cryo-EM images of liposomes formed inside 60 nm DNA rings after purification. **c**, Representative TEM images of liposomes formed inside 29, 46, 60 and 94 nm DNA rings after purification. For each ring size, a cartoon model is shown on the left, with corresponding TEM images on the right. Note that the cartoon models are drawn to scale with respect to one another. **d**, Size distribution of templated versus extruded liposomes measured from negative-stain TEM images. Histograms of five liposome species are normalized to the same scale and fitted to Gaussian distribution curves. Fitting results (mean±s.d., weight) and sample size (*N*) are noted in the insets. Scale bars, 50 nm.

critically on the presence of the lipid molecules initially attached to the inside of the DNA ring.

Transmission electron microscopy (TEM) was then used to examine each fraction. A set of representative images are shown in Fig. 2a (for more images see Supplementary Figs 5 and 6). Under the negative stain condition, vesicles occupied larger volumes than the DNA-origami rings under the uranium stain layer, thus appearing lighter in the greyscale images. F3 and F4 contained mostly 'templated vesicle' structures, in which each DNA ring appeared to be completely filled with a liposome. Together, these two fractions contained nearly half (~58%) of the DNA rings, meaning that such templated vesicles were the main product. The by-products included DNA rings attached to bigger and/or multiple liposomes (found in F2) and rings with smaller liposomes (found in F5–F7). The size distribution of liposomes in F2 to F7 is shown in Supplementary Fig. 6. It is worth noting that the appearance of the vesicles varied considerably across different areas on the TEM grid, ranging from a uniformly white circle to a cup-like shape (edges brighter than the centre). This is probably due to the unevenness of the stain and vesicle dehydration during TEM sample preparation; both are common effects known to be associated with the negative-stain TEM techniques[35,37].

Using cryo-electron microscopy (cryo-EM), we confirmed that the templated liposomes were spherical and unilamellar. On the cryo-specimen grid, a thin layer of sample was rapidly frozen in amorphous ice (thickness of ~110–140 nm), which preserved the nanostructures in three-dimensional space without staining or fixing[38,39]. The DNA-ring templated liposomes were observed in their hydrated state through various EM projections. To enhance contrast, cryo-EM images were taken with two defocuses and merged by a computer program[40]. As shown in Fig. 2b, the membranes appeared as dark annuli with widths of 5.28 ± 0.54 nm, regardless of the EM projection, proving that the liposomes were spherical and unilamellar. However, the DNA rings surrounding the liposomes appeared as light grey tracks with different shapes (for example, line, ellipse and circle) depending on the EM projection angles, consistent with our design. In many cases, the DNA ring appeared to occupy the equatorial plane of the liposome, much like the shape of Saturn. The vesicle size was measured to be 50.0 ± 4.6 nm (Supplementary Fig. 7) using cryo-EM, which is ~8 nm smaller than that measured by negative-stain TEM (58.1 ± 8.3 nm). This small discrepancy can be attributed to vesicle dehydration and deformation during the negative stain process.

We applied similar protocols for sample preparation, purification and characterization to the other three DNA rings with inner diameters of 29, 46 and 94 nm. Gel electrophoresis (Supplementary Fig. 5) and TEM analyses (Fig. 2c and Supplementary Fig. 8) confirmed that the main product in each case was the templated liposome, with its diameter closely matching the inner diameter of the DNA ring (22.1 ± 2.5 nm, 45.5 ± 4.4 nm and 94.6 ± 7.4 nm). We further confirmed the homogeneity of the templated vesicles by fitting their measured diameter histograms with Gaussian distribution curves (Fig. 2d). In each case, at least 85% of the liposomes were within a homogeneous population with the expected size, and

© 2016 Macmillan Publishers Limited. All rights reserved

Table 1 | Buoyant density of the vesicles (60 nm ring template) affected by lipid composition.

Composition	DOPC (%)	DPPC (%)	Cholesterol (%)	Rhod-PE (%)	PEG-2k-PE (%)	DOPS (%)	DOTAP (%)	Main product*,†
0	79.2	-	-	0.8	5	15	-	F3 and F4
1	84.2	-	-	0.8	-	15	-	F2 and F3
2	99.2	-	-	0.8	-	-	-	F2 and F3
3	89.2	-	-	0.8	-	-	10	F1 and F2
4	-	49.2	30	0.8	5	15	-	F3 and F4

DOPC, 1,2-dioleoyl-*sn*-glycero-3-phosphocholine; DPPC, 1,2-dipalmitoyl-*sn*-glycero-3-phosphocholine; Rhod-PE, 1,2-dioleoyl-*sn*-glycero-3-phosphoethanolamine-*N*-(lissamine rhodamine B sulfonyl) (ammonium salt); PEG-2k-PE, 1,2-dioleoyl-*sn*-glycero-3-phosphoethanolamine-*N*-[methoxy(polyethylene glycol)-2000] (ammonium salt); DOPS, 1,2-dioleoyl-*sn*-glycero-3-phospho-L-serine (sodium salt); DOTAP, 1,2-dioleoyl-3-trimethylammonium-propane (chloride salt). *Fractions are numbered 1 to 12 from top to bottom of the density gradient (lightest fraction on top); †DNA ring-to-lipid ratio ≈ 1:188,000.

only a minor population (<15%) appeared to be smaller in diameter, possibly due to contamination during fractionation. Compared to liposomes generated by the traditional extrusion method (Supplementary Fig. 9), these DNA-nanostructure templated liposomes feature size predictability (liposome diameter matches better with the design) and superior monodispersity (a more homogeneous population with smaller standard deviation). See Supplementary section 'Technical Notes' for a comparison of monodispersity with other established methods.

To test the versatility of our method, we made liposomes using the same 60 nm ring as template but with different lipid compositions. As shown in Table 1, the cylindrical and electrically neutral lipid 1,2-dioleoyl-*sn*-glycero-3-phosphocholine (DOPC) was used as the main lipid source for most conditions. The results presented in Fig. 2 were produced using ~80% DOPC, 5% PEG-2k-PE and 15% 1,2-dioleoyl-*sn*-glycero-3-phospho-L-serine (DOPS) (composition 0). With the lipid-to-DNA ring ratio remaining the same, replacing PEG-2k-PE with DOPC (composition 1) resulted in main products with slightly smaller buoyant density, as characterized by isopycnic centrifugation. Using nearly 100% DOPC (composition 2) resulted in products with almost the same buoyant density as those made from composition 1. Furthermore, with ~90% DOPC and 10% positively charged 1,2-dioleoyl-3-trimethylammonium-propane (DOTAP) (composition 3), products were shifted to even lighter fractions in the density gradient (Supplementary Fig. 10). TEM analyses revealed that these products with smaller buoyant density were DNA–membrane complexes with liposomes larger than the DNA rings. Therefore, lipid composition significantly affects the yield of the templated liposomes. In particular, a lipid with bulky (for example, PEG-2k-PE) or negatively charged (for example, phosphatidylserine) head groups appears to limit the overgrowth of the liposome, while a positively charged lipid (for example, DOTAP) does the opposite. However, the yield of templated liposomes can be rescued for lipid compositions 1, 2 and 3 when the lipid-to-DNA ring ratio is reduced to half (that is, ~94,000:1, Supplementary Fig. 10). Thus the lipid concentration may also affect liposome formation kinetics and outcome. We also replaced the DOPC in composition 0 with the high-transition-temperature lipid DPPC and cholesterol, and were able to generate templated liposomes with a comparable yield (composition 4 in Table 1 and Supplementary Fig. 10). Thus the DNA-templated vesicle assembly approach is deemed effective in producing size-controlled liposomes across a range of lipid compositions.

We further demonstrated that the DNA ring can be enzymatically removed from the templated liposome with minimal effect on liposome size. As shown in Supplementary Fig. 11, the liposomes formed inside the 60 nm rings remained largely unchanged (63.0 ± 9.1 nm versus 58.1 ± 8.3 nm) after ring removal by DNaseI. The slight (~8%) increase in observed diameter can be attributed to a more severe liposome deformation without the DNA template during TEM sample preparation. Liposomes made of composition 0 (containing 5% PEG-2k-PE) maintained their homogeneity for 2 weeks with or without the DNA template, but liposomes made of composition 1 (containing no PEG-2k-PE) aggregated and fused within 4 h after template removal (Supplementary Fig. 11). Therefore, liposome stability appears to be governed by the steric protection (repulsion) posed by PEG-2k-PE and the van der Waals attraction between zwitterionic DOPC molecules. Such vesicle stability dependency on lipid composition is consistent with previous reports[41–43].

After producing monodispersed liposomes with pre-defined sizes, we studied the DNA-ring templated liposome formation mechanism using two approaches. First, the stoichiometry and spatial positioning of the anti-handle-modified lipid molecules relative to the DNA ring were systematically varied and the subsequent changes in the liposome formation were characterized. Second, the dialysis process was stopped at various time points to capture critical intermediates during membrane self-assembly.

The modularity and addressability of the DNA-origami structure allowed us to readily change the number and position of the DNA handles (and hence the anti-handle-modified lipid). For instance, variants of the 60 nm ring can be designed to carry 0–16 inner handles for lipid attachment. As described above, rings without inner handles resulted in no association between the ring and vesicle. Furthermore, the vesicle formation results were compared among rings bearing 2, 4, 8 and 16 pre-attached lipid molecules (lipid seeds) inside. The quantities of DNA rings in F1–F7 after isopycnic centrifugation are plotted in Fig. 3a. It is obvious that the yield of a ring with a liposome of desired size (F3 and F4) correlates positively with the number of lipid seeds inside the ring. For example, a ring with two lipid seeds gave merely 23% yield of desired product, a dramatic decrease from the 58% yield achieved by the ring with 16 seeds. Variants with different inner handles were designed based on the 46 nm ring and the same trend was confirmed (Supplementary Fig. 12). Next, the position of the lipid seed was changed from the distal end to the proximal end of the handle/anti-handle duplex to bring the seeds closer to the 29 nm DNA ring. This change shifted the mean diameter of liposomes in F5 (the fraction containing the most DNA rings, Supplementary Fig. 13) from 14 to 22 nm, matching well with the cartoon models shown in Fig. 3b, where the lipid-modified duplexes were considered as rigid rods. The lipid seed position was then changed from the inside to the outside of the ring. This was achieved by placing the handles on different DNA double helices of the ring (Fig. 3c). Four variants of the 46 nm ring were constructed for this purpose, each carrying three handles forming 0°, 60°, 120° or 180° angles with the ring. With the lipid seeds inside (handles at 0° and 60°), most of the rings had liposomes formed within their boundaries, promoting the formation of templated liposomes. In contrast, with the handles flipped (180° and 120°), most rings had liposomes formed outside, causing the formation of aggregates. To illustrate this difference, the number of liposomes associated with a ring in one of the density gradient fractions (F4) is plotted in Fig. 3c (for more images see Supplementary Fig. 14). It is obvious that the rings with lipid seeds inside favoured the formation of a single liposome per ring, and those with lipid seeds outside yielded a significant amount of three well-separated liposomes surrounding a ring. These findings led us to the hypothesis that

© 2016 Macmillan Publishers Limited. All rights reserved

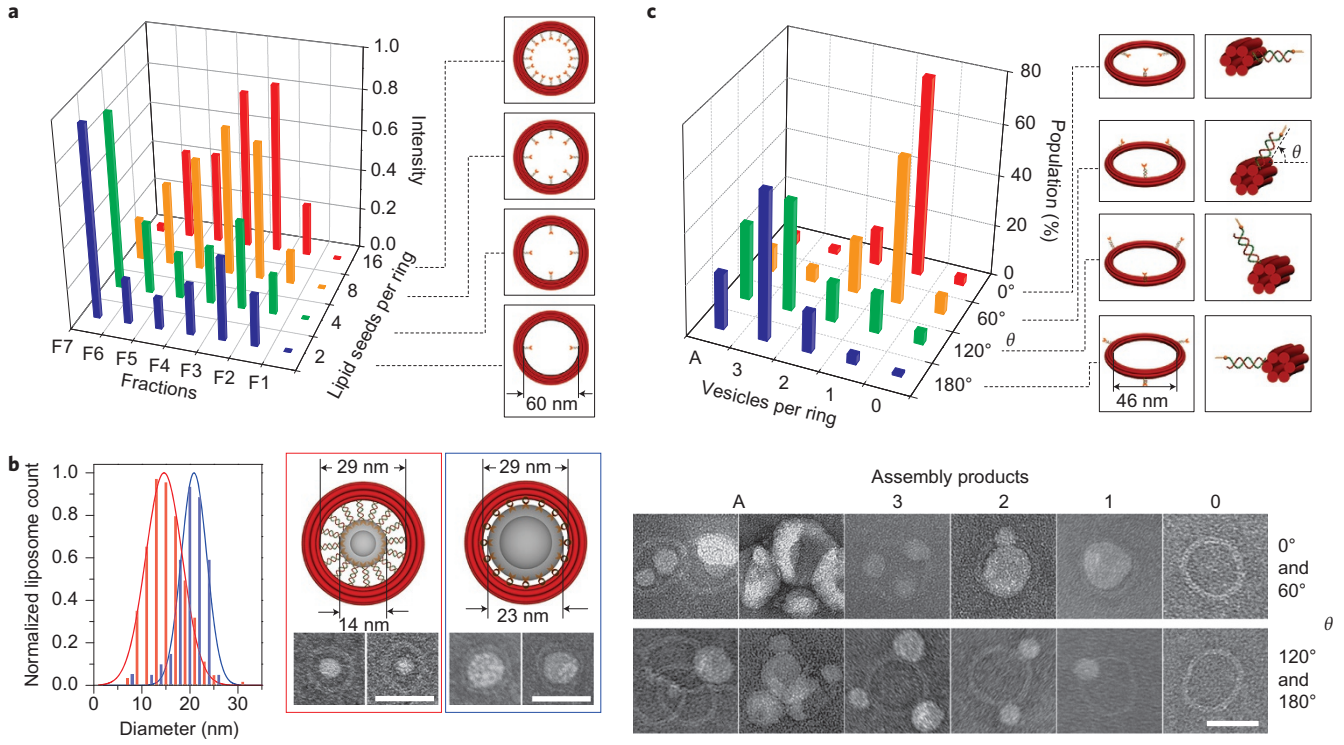


Figure 3 | Effect of initial lipid seed placement on final vesicle formation. a, Lipid seed number inside a 60 nm ring versus the yield of size-controlled liposomes. The three-dimensional bar graph is plotted based on the amount of DNA in each post-centrifugation fraction as measured by the DNA band intensity after gel electrophoresis. F3 and F4 contain liposomes with a designated size. Cartoon models of the four DNA ring constructs are shown on the right of the bar graph. **b**, A comparison between two 29 nm rings with lipid seeds placed at different distances away from the inner edge of the ring. Representative TEM images and size distribution histograms (N = 298, red; N = 69, blue) are taken from the fraction that contained the most DNA rings. **c**, Vesicles assembled on 46 nm rings with lipid seeds inside or outside the ring. The assembly products are sorted into five categories based on the number of vesicles per ring (A, aggregates). Representative TEM images of each category are shown (bottom) and the occurrences of all types of product are plotted as a three-dimensional bar graph. Data are taken from the same fraction for all four ring species. Scale bars, 50 nm.

the self-assembly of templated vesicles is initially nucleated by the lipid seeds and is finally restricted by the rigid body of the DNA-origami ring.

To test our hypothesis, we performed a second set of experiments to capture the intermediate structures during liposome formation. Based on previous mechanistic studies of vesicle reconstitution from lipid–detergent micelles[44–48], we reasoned that the formation of the templated vesicles completes during the dialysis of OG. To determine the important time points of dialysis, radioactive OG was used to track the amount of detergent remaining at 0, 0.5, 1, 3, 3.5, 5 and 16 h. As shown in Fig. 4a, the change in detergent concentration followed a single exponential curve. After 1 h of dialysis, the OG in the lipid–detergent mixture was diluted to 0.093%, equivalent to ~20% of the CMC; after 3 h, the OG level dropped to background. We thus imaged samples after 0, 0.5, 1, 1.5 and 16 h dialysis and further categorized the DNA rings based on their lipid/detergent association states. For the purpose of this study, only the rings with clear boundaries were included for statistics (for example, rings covered by larger lipid/detergent aggregates were not counted).

We performed such a mechanistic study on 60 nm rings and again systematically varied the number of lipid seeds inside each ring (0, 4, 8 and 16). As expected, DNA-rings without lipid seeds remained empty throughout the dialysis (data not shown). For the ring initially modified with four lipid molecules, the observations (Fig. 4b) are as follows. Without dialysis (0.67% OG), rings lacked noticeable lipid attachment. After 30 min of dialysis (0.23% OG), in addition to such empty DNA structures, the rings appeared to be decorated with a substantial amount of lipid. The DNA–lipid association at this stage mainly took two forms: most of the DNA rings bore a strip of worm-like lipid–detergent micelle (mean thickness = 5.2 nm) on the inside, but some of the DNA rings appeared to be wrapped tightly by a continuous lipid bilayer (see Supplementary Fig. 15 for more images). At 1 h (0.093% OG), the population of empty rings decreased further, and more rings appeared to be associated with worm-like micelles or wrapped by a continuous bilayer. After 1.5 h dialysis (0.037% OG), aside from these intermediates, about one-third of the DNA rings started to attach with one to four separated vesicles (mean diameter = 18 nm) on the inside. A small population of rings each fully filled with a liposome (Saturn-like structures) also emerged. Finally, with detergent completely removed after overnight dialysis, the majority of rings were either fully filled with a single liposome or associated with a few separate vesicles, and only a minority of rings remained empty. Other structures found at 0.5, 1 and 1.5 h were almost completely absent from the detergent-free mixture. When the number of lipid seeds per ring was changed to 8 and 16, similar observations were made, with two exceptions after 1.5 h of dialysis. First, in addition to associating with individual small liposomes, rings modified with 8 or 16 lipid seeds encompassed a toroidal membrane structure with a mean section diameter of 15 nm. Second, compared with rings having four lipid seeds, more rings were fully filled after 1 h of dialysis. This difference became more obvious after 1.5 h and eventually resulted in a higher percentage of size-controlled liposomes in the final detergent-free mixture, which is consistent with our findings in Fig. 3a.

Although extreme care has to be taken when interpreting the negative-stain TEM data, the following trends are obvious from

© 2016 Macmillan Publishers Limited. All rights reserved

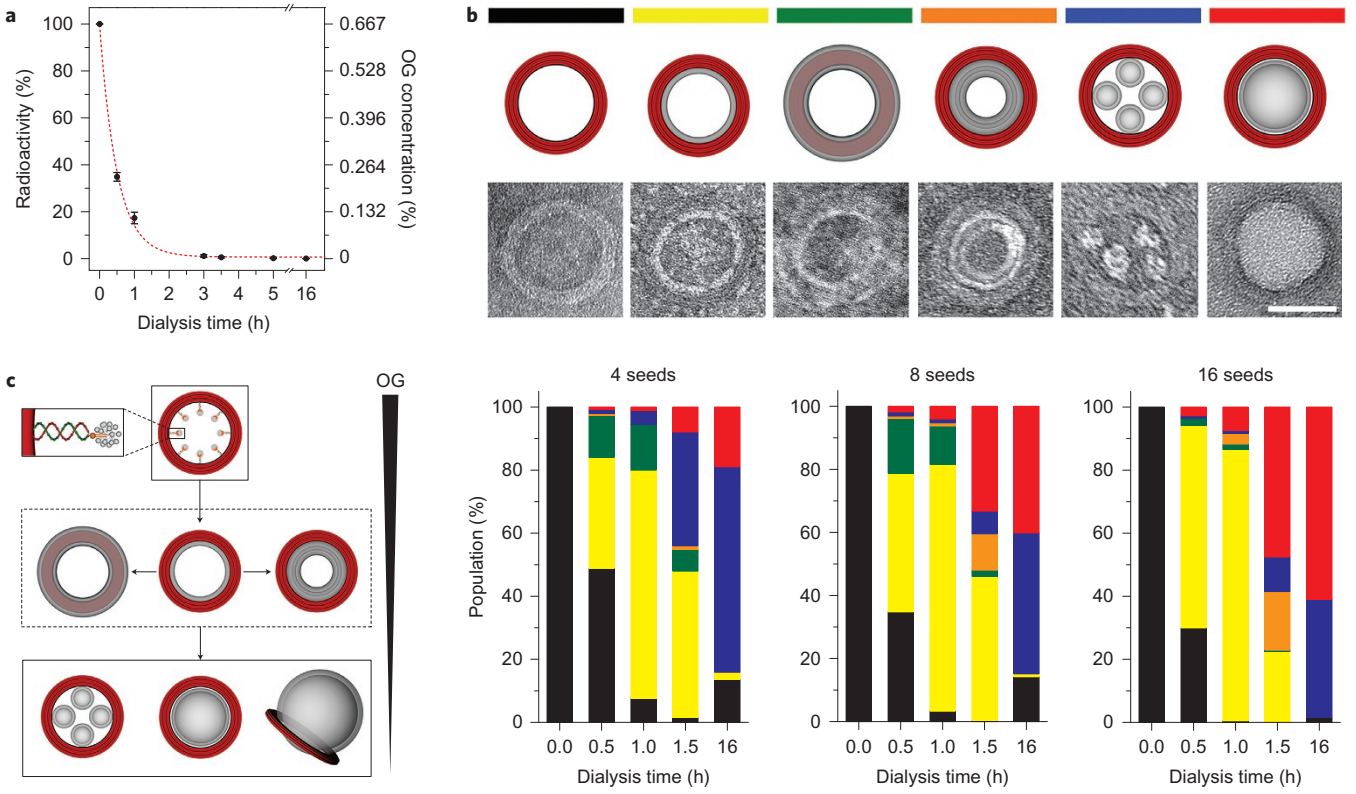


Figure 4 | Vesicle formation mechanism studied by capturing intermediates during dialysis. a, Detergent removal monitored by the remaining radioactivity of ^{14}C-labelled OG at different time points. Error bars represent s.d. of two to four measurements. Dotted line is a fit using a single-exponential decay curve. **b**, Top: summary of the intermediates and final products. Cartoon models (lipid seeds are not drawn for clarity) and their colour codes (as used in the bar graphs below) are shown above their corresponding TEM images. Scale bar, 50 nm. Bottom: quantitative measure of all structures found at different time points (0, 0.5, 1, 1.5 and 16 h) during dialysis of rings with 4, 8 and 16 lipid seeds inside ($273 \geq N \geq 85$). **c**, Schematic illustrating the hypothesized mechanism of size-controlled liposome formation templated by a DNA ring. Cartoon models of starting material, intermediates and final products are shown in the top, middle and bottom rows, respectively.

the mechanistic study. First, the association between the DNA ring and lipid bilayer depends on the presence of lipid seeds, confirming their role as nucleation points. Second, the total mass of lipid associated with a ring increases continuously as the detergent concentration decreases, suggesting a gradual growth process as opposed to the direct capture of a liposome. Third, the formation of size-controlled liposomes (Saturn-like structures) accelerates when more lipid molecules are initially placed on the ring, suggesting that faster bilayer growth and merger can be driven by a higher number of nucleation sites packed in a confined space. These findings strongly support our hypothesis of templated liposome formation (Fig. 4c): the lipid seeds inside the DNA ring are initially stabilized by small clusters of lipid–detergent micelles (Fig. 4c, top row); as the detergent concentration decreases, they merge and expand in one dimension to form worm-like micelles, which further expand in two dimensions and curve up (in three dimensions) to form lipid–bilayer structures resembling a doughnut (Fig. 4c, middle row); such intermediates become unstable when detergent is further diluted and eventually lead to the formation of liposomes inside the ring (Fig. 4c, bottom row). The Saturn-like structures are favoured when a high density of seeds are present within a rigid DNA frame.

Discussion

In summary, we have presented a strategy to generate small unilamellar vesicles (SUVs) by nanotemplating. The programmable vesicle size, outstanding vesicle monodispersity and versatility to produce SUVs with different lipid compositions are the most valuable features of this system. In addition, the liposomes self-assemble during a simple detergent removal process (for example, through dialysis, as demonstrated here, or by direct dilution/adsorption as explored by others[46,48]), making this method easily accessible to the general research community and more importantly, compatible for loading cargos such as nucleic acids, antibodies and small molecules[4]. Other natural and synthetic amphipathic molecules could in principle be incorporated to functionalize and varietize the vesicles. The virtually complete OG depletion and the decent vesicle stability (lipid composition 0) are promising features that point to an outstanding membrane integrity[5,46]. However, unlike a template-free vesicle formation process, here the DNA nanotemplate dictates the outcome of membrane self-assembly by providing a nucleation site to start lipid aggregation, a rigid structure to confine the vesicle growth, and an added mass to facilitate purification. In this Article we have focused on producing sub-100-nm vesicles at an analytical scale (up to ~100 μl of 0.9 mM lipid) to prove the concept. However, with the availability of three-dimensional DNA nanostructures larger than 100 nm (refs 49,50), it is conceivable that this nanotemplating technique could be generalized to make large unilamellar vesicles with similar features. We note that this technique requires much improvement in terms of cost efficiency, lipid recovery rate and scalability to meet the needs of many biomedical applications (see Supplementary section 'Technical Notes' for further discussion). However, the method in its current form serves adequately to probe the mechanism of nucleated liposome growth and holds great promise for studying protein behaviour on membranes with defined curvatures.

In biological cells, membranes appear with different shapes and constantly change their chemical and physical properties to

© 2016 Macmillan Publishers Limited. All rights reserved

accommodate the cell's needs, for growth, division, communication and to maintain homeostasis. Now that we have established a method to guide membrane formation *in vitro* by means of DNA nanotemplates, in our future studies we aspire to better understand and mimic this elegance of nature. For example, membrane-deforming proteins (for example, SNARE and BAR-domain proteins) could be organized on the DNA template to mediate membrane remodelling and rigorously study protein–membrane interactions. Also, vesicles with non-spherical (for example, tubular) shapes could be constructed using designer DNA templates. Moreover, reconfigurable DNA structures may be built to deform the membrane in a stepwise, controlled manner. Finally, more advanced membrane manipulation techniques based on a similar concept could open up new opportunities in biotechnology such as targeted drug delivery across a membrane barrier and programmable neuron communication.

Methods

Preparation of lipidated DNA anti-handles. Thiol-modified DNA oligonucleotides (Integrated DNA Technologies) were treated with tris(2-carboxyethyl)phosphine (Sigma-Aldrich) for 30 min (20 nmol DNA per reaction) and immediately reacted with 0.4 μmol of 18:1 MPB PE (Avanti Polar Lipids) in aqueous solutions containing ~2% OG (EMD Millipore) at room temperature for 45 min. The reaction mixture was then diluted twofold, added to 0.6 μmol pre-dried lipids, agitated, and dialysed overnight to incorporate lipidated DNA molecules into liposomes. The conjugation products were separated from unconjugated DNA via isopycnic centrifugation in iodixanol gradients (Cosmo Bio USA) and later analysed by SDS–polyacrylamide gel electrophoresis.

DNA-origami ring design and preparation. The DNA-origami rings were designed using caDNAno (caDNAno.org). Inner- and outer-handle sequences (21 nt) were generated by NUPACK (nupack.org) and manually added to the 3′-ends of the appropriate staple strands. DNA scaffold strands (3,024, 7,308, 7,560 or 8,064 nt) were produced using *E. coli* and M13-derived bacteriophages. Staple strands were synthesized by Integrated DNA Technologies. The DNA rings were assembled from a scaffold strand (50 nM) and a pool of staple strands (300 nM each) in 5 mM Tris HCl, 1 mM EDTA, pH 8.0 with 10 or 12 mM of $MgCl_2$ using a 36 h thermal annealing programme. Correctly assembled DNA nanostructures were purified via rate-zonal centrifugation in glycerol gradients as described previously[36].

Preparation of DNA-ring templated liposomes. DNA rings were first labelled with lipidated anti-inner handles and Cy5-modified anti-outer handles in one-pot hybridization mixtures containing 1% OG. To form DNA-ring templated liposomes, 15 μl 1× hydration buffer (25 mM HEPES, 400 mM KCl, 10 mM $MgCl_2$, pH 7.5) and 5 μl 15 mM rehydrated lipid mixture (compositions shown in Table 1) were added to 40 μl 10 nM lipid- and Cy5- labelled DNA rings. The solution was gently shaken for 30 min at room temperature, diluted with 60 μl 1× hydration buffer containing 0.67% OG, put into a 7 kDa molecular weight cutoff dialysis cassette (Thermo Scientific) and dialysed against 2 l 1× hydration buffer for 16 h. The dialysed solutions were subjected to isopycnic centrifugation in iodixanol gradients. Recovered fractions were analysed by SDS–agarose gel electrophoresis to determine their contents. Optionally, DNase I (Thermo Scientific) was used to remove DNA rings according to the manufacturer's recommendation.

Electron microscopy. Negative staining was achieved by adsorbing ~5 μl sample on a glow-discharged formvar/carbon-coated copper grid (Electron Microscopy Sciences) and staining with 2% uranyl formate. Imaging was performed on a JEOL JEM-1400 Plus microscope operated at 80 kV. Samples for cryo-EM were first concentrated using centrifugal filters with 30 kDa nominal molecular weight limit (EMD Millipore) to remove iodixanol and achieve ~50 nM DNA-ring concentration. The concentrated samples were then adsorbed on glow-discharged holey carbon grids (Quantifoil MicroTools), which were subsequently washed with buffer solution with 10% reduced salt concentration, blotted, and flash frozen in liquid ethane using FEI Vitrobot. Imaging was performed on an FEI Tecnai-F20 microscope operated at 200 kV.

Time-course study of liposome formation. To determine the remaining OG concentration at various time points during dialysis, 1.8 μl of ~0.01% ^{14}C-labelled OG (American Radiolabeled Chemicals) were added to a 360 μl solution containing ~6.7 nM lipid-labelled DNA ring, ~2.5 mM extra lipid and 0.67% non-radioactive OG. After 1 h agitation, 10 μl of mixture was set aside, and the rest was diluted to ~760 μl in 1× hydration buffer with 0.67% non-radioactive OG and split into six cassettes for dialysis against 1× hydration buffer. Using a scintillation counter (Beckmann-Coulter), the radioactivity of the mixture after 0, 0.5, 1, 3, 3.5, 5 or 16 h of dialysis was measured. The remaining OG concentrations were then calculated based on those measurements. To capture intermediates during detergent removal, a similar liposome formation protocol was used with non-radioactive OG and the dialysis was stopped after 0, 0.5, 1, 1.5 or 16 h. Such dialysed solutions were fractionated after isopycnic centrifugation and characterized by SDS–agarose gel electrophoresis and negative-stain TEM. Gel and TEM images were analysed manually using ImageJ (National Institutes of Health).

Received 28 August 2015; accepted 3 February 2016; published online 21 March 2016

References

1. Cho, W. & Stahelin, R. V. Membrane–protein interactions in cell signaling and membrane trafficking. *Annu. Rev. Biophys. Biomol. Struct.* **34,** 119–151 (2005).
2. Rigaud, J.-L. & Lévy, D. Reconstitution of membrane proteins into liposomes. *Methods Enzymol.* **372,** 65–86 (2003).
3. Bally, M. *et al.* Liposome and lipid bilayer arrays towards biosensing applications. *Small* **6,** 2481–2497 (2010).
4. Allen, T. M. & Cullis, P. R. Liposomal drug delivery systems: from concept to clinical applications. *Adv. Drug Deliv. Rev.* **65,** 36–48 (2013).
5. Çağdaş, M., Sezer, A. D. & Bucak, S. *Liposomes as Potential Drug Carrier Systems for Drug Delivery* (InTech, 2014).
6. Dua, J., Rana, A. & Bhandari, A. Liposome: methods of preparation and applications. *Int. J. Pharm. Stud. Res.* **3,** 14–20 (2012).
7. Gregory, G. *Liposome Technology* Vol. 1 (CRC, 2006).
8. Batzri, S. & Korn, E. D. Single bilayer liposomes prepared without sonication. *Biochim. Biophys. Acta* **298,** 1015–1019 (1973).
9. Bosworth, M. E., Hunt, C. A. & Pratt, D. Liposome dialysis for improved size distributions. *J. Pharm. Sci.* **71,** 806–812 (1982).
10. Mayer, L. D., Hope, M. J., Cullis, P. R. & Janoff, A. S. Solute distributions and trapping efficiencies observed in freeze-thawed multilamellar vesicles. *Biochim. Biophys. Acta* **817,** 193–196 (1985).
11. Pidgeon, C., McNeely, S., Schmidt, T. & Johnson, J. E. Multilayered vesicles prepared by reverse-phase evaporation: liposome structure and optimum solute entrapment. *Biochemistry* **26,** 17–29 (1987).
12. Genc, R., Ortiz, M. & O'Sullivan, C. K. Curvature-tuned preparation of nanoliposomes. *Langmuir* **25,** 12604–12613 (2009).
13. Mouritsen, O. G. Lipids, curvature, and nano-medicine. *Eur. J. Lipid Sci. Technol.* **113,** 1174–1187 (2011).
14. Sun, J. *et al.* Tunable rigidity of (polymeric core)–(lipid shell) nanoparticles for regulated cellular uptake. *Adv. Mater.* **27,** 1402–1407 (2015).
15. Schubert, R. Liposome preparation by detergent removal. *Methods Enzymol.* **367,** 46–70 (2003).
16. Holzer, M., Barnert, S., Momm, J. & Schubert, R. Preparative size exclusion chromatography combined with detergent removal as a versatile tool to prepare unilamellar and spherical liposomes of highly uniform size distribution. *J. Chromatogr. A* **1216,** 5838–5848 (2009).
17. Huang, C. Studies on phosphatidylcholine vesicles. Formation and physical characteristics. *Biochemistry* **8,** 344–352 (1969).
18. Olson, F., Hunt, C. A., Szoka, F. C., Vail, W. J. & Papahadjopoulos, D. Preparation of liposomes of defined size distribution by extrusion through polycarbonate membranes. *Biochim. Biophys. Acta* **557,** 9–23 (1979).
19. Hope, M. J., Bally, M. B., Webb, G. & Cullis, P. R. Production of large unilamellar vesicles by a rapid extrusion procedure: characterization of size distribution, trapped volume and ability to maintain a membrane potential. *Biochim. Biophys. Acta* **812,** 55–65 (1985).
20. Silva, R., Ferreira, H., Little, C. & Cavaco-Paulo, A. Effect of ultrasound parameters for unilamellar liposome preparation. *Ultrason. Sonochem.* **17,** 628–632 (2010).
21. Wang, T., Wang, N., Wang, T., Sun, W. & Li, T. Preparation of submicron liposomes exhibiting efficient entrapment of drugs by freeze-drying water-in-oil emulsions. *Chem. Phys. Lipids* **164,** 151–157 (2011).
22. Yu, D. G. *et al.* Self-assembled liposomes from amphiphilic electrospun nanofibers. *Soft Matter* **7,** 8239–8247 (2011).
23. Jahn, A., Lucas, F., Wepf, R. A. & Dittrich, P. S. Freezing continuous-flow self-assembly in a microfluidic device: toward imaging of liposome formation. *Langmuir* **29,** 1717–1723 (2013).
24. McMahon, H. T. & Gallop, J. L. Membrane curvature and mechanisms of dynamic cell membrane remodelling. *Nature* **438,** 590–596 (2005).
25. Langecker, M., Arnaut, V., List, J. & Simmel, F. C. DNA nanostructures interacting with lipid bilayer membranes. *Acc. Chem. Res.* **47,** 1807–1815 (2014).
26. Beales, P. A. & Vanderlick, T. K. Specific binding of different vesicle populations by the hybridization of membrane-anchored DNA. *J. Phys. Chem. A* **111,** 12372–12380 (2007).
27. Chan, Y. H., van Lengerich, B. & Boxer, S. G. Effects of linker sequences on vesicle fusion mediated by lipid-anchored DNA oligonucleotides. *Proc. Natl Acad. Sci. USA* **106,** 979–984 (2009).
28. Dave, N. & Liu, J. Programmable assembly of DNA-functionalized liposomes by DNA. *ACS Nano* **5,** 1304–1312 (2011).
29. Pinheiro, A. V., Han, D., Shih, W. M. & Yan, H. Challenges and opportunities for structural DNA nanotechnology. *Nature Nanotech.* **6,** 763–772 (2011).

© 2016 Macmillan Publishers Limited. All rights reserved

30. Jones, M. R., Seeman, N. C. & Mirkin, C. A. Nanomaterials. Programmable materials and the nature of the DNA bond. *Science* **347,** 1260901 (2015).
31. Rothemund, P. W. Folding DNA to create nanoscale shapes and patterns. *Nature* **440,** 297–302 (2006).
32. Dietz, H., Douglas, S. M. & Shih, W. M. Folding DNA into twisted and curved nanoscale shapes. *Science* **325,** 725–730 (2009).
33. Li, P. *et al.* A pH-sensitive multifunctional gene carrier assembled via layer-by-layer technique for efficient gene delivery. *Int. J. Nanomed.* **7,** 925–939 (2012).
34. Dong, Y. *et al.* Frame-guided assembly of vesicles with programmed geometry and dimensions. *Angew. Chem. Int. Ed.* **53,** 2607–2610 (2014).
35. Perrault, S. D. & Shih, W. M. Virus-inspired membrane encapsulation of DNA nanostructures to achieve *in vivo* stability. *ACS Nano* **8,** 5132–5140 (2014).
36. Lin, C., Perrault, S. D., Kwak, M., Graf, F. & Shih, W. M. Purification of DNA-origami nanostructures by rate-zonal centrifugation. *Nucleic Acids Res.* **41,** e40 (2013).
37. Kourembanas, S. Exosomes: vehicles of intercellular signaling, biomarkers, and vectors of cell therapy. *Annu. Rev. Physiol.* **77,** 13–27 (2015).
38. Vinson, P. K., Talmon, Y. & Walter, A. Vesicle–micelle transition of phosphatidylcholine and octyl glucoside elucidated by cryo-transmission electron-microscopy. *Biophys. J.* **56,** 669–681 (1989).
39. Cho, H.-J. *et al.* Measurement of ice thickness on vitreous ice embedded cryo-EM grids: investigation of optimizing condition for visualizing macromolecules. *J. Anal. Sci. Technol.* **4,** 7 (2013).
40. Ludtke, S. J. & Chiu, W. Focal pair merging for contrast enhancement of single particles. *J. Struct. Biol.* **144,** 73–78 (2003).
41. Kaler, E. W., Murthy, A. K., Rodriguez, B. E. & Zasadzinski, J. A. Spontaneous vesicle formation in aqueous mixtures of single-tailed surfactants. *Science* **245,** 1371–1374 (1989).
42. Li, W., Huang, Z., MacKay, J. A., Grube, S. & Szoka, F. C. Jr. Low-pH-sensitive poly(ethylene glycol) (PEG)-stabilized plasmid nanolipoparticles: effects of PEG chain length, lipid composition and assembly conditions on gene delivery. *J. Gene Med.* **7,** 67–79 (2005).
43. Li, W. & Szoka, F. C. Jr. Lipid-based nanoparticles for nucleic acid delivery. *Pharm. Res.* **24,** 438–449 (2007).
44. Ollivon, M., Lesieur, S., Grabielle-Madelmont, C. & Paternostre, M. Vesicle reconstitution from lipid–detergent mixed micelles. *Biochim. Biophys. Acta* **1508,** 34–50 (2000).
45. Stuart, M. C. & Boekema, E. J. Two distinct mechanisms of vesicle-to-micelle and micelle-to-vesicle transition are mediated by the packing parameter of phospholipid–detergent systems. *Biochim. Biophys. Acta* **1768,** 2681–2689 (2007).
46. Mimms, L. T., Zampighi, G., Nozaki, Y., Tanford, C. & Reynolds, J. A. Phospholipid vesicle formation and transmembrane protein incorporation using octyl glucoside. *Biochemistry* **20,** 833–840 (1981).
47. Zumbuehl, O. & Weder, H. G. Liposomes of controllable size in the range of 40 to 180 nm by defined dialysis of lipid/detergent mixed micelles. *Biochim. Biophys. Acta* **640,** 252–262 (1981).
48. Philippot, J., Mutaftschiev, S. & Liautard, J. P. A very mild method allowing the encapsulation of very high amounts of macromolecules into very large (1000 nm) unilamellar liposomes. *Biochim. Biophys. Acta* **734,** 137–143 (1983).
49. Iinuma, R. *et al.* Polyhedra self-assembled from DNA tripods and characterized with 3D DNA-PAINT. *Science* **344,** 65–69 (2014).
50. Gerling, T., Wagenbauer, K. F., Neuner, A. M. & Dietz, H. Dynamic DNA devices and assemblies formed by shape-complementary, non-base pairing 3D components. *Science* **347,** 1446–1452 (2015).

Acknowledgements

The authors thank P.D. Ellis for designing the DNA rings used for placing lipid seeds at different angles and for proofreading the manuscript, and F. Sigworth for providing cryo-electron micrographs of extruded liposomes. This work is supported by a National Institutes of Health (NIH) Director's New Innovator Award (DP2-GM114830), an NIH grant (R21-GM109466) and a Yale University faculty startup fund to C.L., an NIH grant to J.E.R. (R01-DK027044) and an NIH Director's New Innovator Award (DP2-OD004641), an Army Research Office MURI grant (W911NF-12-1-0420), National Science Foundation Expeditions Grant (1317694) and a Wyss Institute for Biologically Inspired Engineering Faculty Award to W.M.S.

Author contributions

Y.Y. and J.W. designed and conducted the majority of the experiments, analysed the data, prepared the majority of the manuscript and contributed equally to this work. H.S. performed cryo-EM studies and prepared the manuscript. W.X. initiated the project, developed the DNA–lipid conjugation method and designed and performed pilot experiments to prepare and purify DNA-ring enclosed vesicles. W.M.S. initiated the project and discussed the results. J.E.R. initiated the project, supervised J.W. and W.X., and discussed the results. C.L. initiated the project, designed and supervised the study, interpreted the data and prepared the manuscript. All authors reviewed and approved the manuscript.

Additional information

Supplementary information is available in the online version of the paper. Reprints and permissions information is available online at www.nature.com/reprints. Correspondence and requests for materials should be addressed to W.M.S., J.E.R. and C.L.

Competing financial interests

The authors declare no competing financial interests.

© 2016 Macmillan Publishers Limited. All rights reserved